Time-Dependent Closure of a Borehole in a Viscoplastic Rock

Xiyang Xie[1], Erling Fjær[1,2], and Emmanuel Detournay[3*]

[1]NTNU, [2]SINTEF, and [3]UMN

The paper describes a model to predict and analyze the time-dependent closure of a borehole drilled in a soft rock subjected to an initial isotropic stress, and the build-up of stress on a rigid casing after contact with the deforming rock. The rock behaves as a viscoplastic material characterized by a Mohr-Coulomb yield criterion and plastic potential, and by a time-dependent stress-strain deviatoric response akin to a Bingham rheology. The model formulation recognizes the particular structure of the solution, namely that the borehole is encircled by an evolving viscoplastic annulus, itself surrounded by an infinite domain, where the rock is either elastic or is unloading elastically. Noting that the solution outside the viscoplastic boundary is given explicitly by the Lamé solution, the evolution problem is formulated as an initial boundary value problem in the viscoplastic region only, but with a free boundary — the growing or shrinking interface between the viscoplastic and the elastic domains. The equations governing the mechanical fields and the evolution of viscoplastic boundary are spatially discretized on a moving mesh with a fixed

*Corresponding Author: detou001@umn.edu

number of nodes. The final system of equations is a set of first order ODEs that are efficiently solved using the MATLAB routine ODE45. The numerical simulations reveal (i) the time-dependent deformation and stress state of rock in the viscoplastic annulus before and after the contact, (ii) the time of first contact between the deforming rock and the casing, (iii) the effective duration of the stress build-up on the casing, and (iv) the large time contact pressure, which is well approximated by the elastoplastic solution.

1 Introduction

Potential leakage from deep oil and gas reservoirs through the casing annulus of boreholes, long after production has ceased, represents a serious environmental risk. However, a tight contact between the rock and the casing resulting from the time-dependent deformation of shale around a borehole could in principle contribute to the establishment of a physical barrier that would mitigate or even prevent leakage [Williams et al., 2009, Norsok, 2013].

The critical issues that have to be addressed in regard to the potential seal provided by the shale are the following. (i) How much time is elapsing between drilling and the first contact between the deforming rock and the casing? (ii) What is the effective duration of the stress build-up on the casing? (iii) What is the maximum contact pressure on the casing? In conjunction with a realistic constitutive model of the shale, a theoretical model of the time-dependent response of the rock to drilling and contact with the casing can shed light on these questions.

The model investigated in this paper is constructed on the assumptions that the far-field stress is isotropic, the rock is deforming under plane strain conditions, and the shale behaves as a Bingham viscoplastic material governed by a Mohr-Coulomb criterion in its deviatoric response. This last assumption implies the existence of a viscoplastic annulus around the borehole where progressive failure of the rock takes place, if the yield limit

is exceeded by the elastic stress field around the borehole. Indeed, the stress state in the viscoplastic region can temporarily go beyond the yield criterion. This over-stress, as defined by Perzyna [1966], progressively decreases with developing viscoplastic strain under constant loading, to eventually vanish at large time.

The stress readjustment in the viscoplastic annulus leads to a continued expansion of this region until further closure of the borehole is prevented by the rigid casing. After contact, the build-up of pressure on the rock-casing interface causes a shrinkage of the viscoplastic region, which eventually vanishes when the yield criterion is nowhere violated. Such a large time asymptotic state is characterized by a plastic annulus around the borehole. In the absence of a casing, an equilibrium state is also eventually reached, after continued expansion of the viscoplastic region. A key feature of this problem is thus the existence of a moving boundary that encloses a growing or shrinking viscoplastic annulus depending on the boundary condition at the borehole wall. The moving boundary makes the problem challenging to solve even under the simplifying assumptions of axisymmetry and plane strain.

The assumed viscoplastic constitutive response of shale traces its origin to the Bingham [1922] rheological model and to the Perzyna [1966] over-stress theory. In Perzyna's theory, the stress state can temporarily violate the yield criterion. Various extensions of the original theory of Perzyna [1966] have been proposed, and only some of these works are highlighted in the following (see the comprehensive reviews by Debernardi [2008] and by Hashiguchi [2017]). In Cristescu [1988], the viscoplastic strain is determined as a function of the irreversible stress work. Lemaitre and Chaboche [1990] proposed a viscoplastic constitutive model that takes the strain-dependent hardening into consideration. In their model, the viscoplastic yield criterion is identified with the hydrostatic axis in the principal stress space, implying therefore a long-term equilibrium solution without any shear stress. Malan [1999] described a viscoplastic constitutive model with two yield criteria: one plastic yield criterion for the intact rock and the other viscoplastic yield

criterion for the failed rock. The yield stress has to fulfill the plastic yield criterion first so that the viscoplastic yield criterion can be active and the stress state can return progressively to the viscoplastic yield criterion. Boidy [2002] extended Lemaitre's work by assuming that the viscoplastic yield criterion is a closed surface surrounding the hydrostatic axis. Debernardi [2008] proposed a stress-hardening viscoplastic constitutive model with a plastic yield criterion and a viscoplastic yield criterion (similar to the Malan's model). However, in contrast to Malan's, the viscoplastic yield criterion is always active in Debernardi's model (the stress does not need to reach the yield criterion first to activate the viscoplastic yield criterion).

Applications of the viscoplastic theory to tunnel and borehole problems have been the subject of several investigations using both analytical and numerical techniques. However, the handful of existing analytical solutions [Cristescu, 1988, Fritz, 1984] do not take the evolution of the viscoplastic region into consideration. Most of the studies rely on solving the problem numerically, using the finite difference or the finite element method [Malan, 1999, Boidy et al., 2002, Bonini et al., 2007, Debernardi, 2008, Barla et al., 2012, Moghadam, 2013, Bian et al., 2017]. Although the evolving viscoplastic region plays a critical role in the progressive borehole closure problem, it was only discussed within the context of the finite element method in a few publications [Gioda, 1982, Gioda and Cividini, 1996]. Hence, to our knowledge, no papers describe a solution with an explicit tracking of the moving boundary of the viscoplastic region.

The objective of this contribution is two-fold. First, it is to formulate a mathematical model that enables an explicit tracking of the external radius of the viscoplastic annulus. Such a formulation is the foundation for an efficient computational algorithm that only requires solving for the mechanical fields in the viscoplastic region. Second to perform a parametric analysis to understand the role of the key parameters controlling the borehole closure and the pressure build-up on the casing.

The paper is organized as follows. Section 2 formulates the initial boundary value

problem in the evolving viscoplastic zone. Section 3 introduces the scaling and a dimensionless formulation of the model that relies on mapping the evolving viscoplastic region onto a unit plane. Section 4 describes the finite difference scheme on a moving mesh used to solve the field equations in the viscoplastic region. Section 5 illustrates the simulation results both before and after the rock-casing contact. It also analyzes the influence of a few parameters on the long-term casing contact pressure and on the time it takes to reach the asymptotic value.

2 Mathematical model

2.1 Problem definition

We consider the time-dependent closure of a vertical borehole drilled through viscoplastic rock, as well as the build-up of pressure at the rock-casing interface when the formation closure is further prevented by a rigid casing. To calculate the progressive deformation of the rock around the borehole and the subsequent build-up of pressure on the casing, we assume an isotropic and homogeneous rock and an isotropic far-field stress σ_0 in a plane orthogonal to the borehole. After further assuming plane strain and axisymmetric conditions in this plane (generally horizontal), the problem can be completely formulated in terms of radial displacement $u(r,t)$, principal radial stress $\sigma_r(r,t)$ and principal tangential stress $\sigma_\theta(r,t)$ as functions of radius $r \geq a$, where a is the nominal borehole radius, and time $t \geq 0$. It is also assumed that the out-plane normal stress does not affect the solution of this problem.

We are interested in two phases of this problem, before and after rock-casing contact. The first phase deals with the progressive closure of the borehole before the rock-casing contact. The borehole closure is triggered by drilling, which is modeled here by a sudden drop of radial stress $\sigma_r(a,t)$ at the borehole from the initial value σ_0 (corresponding to a uniform far-field stress in the plane) to a pre-assumed mud pressure p_m (corresponding

to the hydrostatic pressure of the mud column inside the borehole)

$$\sigma_r(a,t) = \sigma_0 - (\sigma_0 - p_m) H(t), \tag{1}$$

with $H(t)$ denoting the Heaviside function (positive stress is assumed in compression). The drilling-induced unloading causes a stress concentration around the borehole. It is assumed the radial stress drop $\sigma_0 - p_m$ is large enough, so that the corresponding elastic stress state violates the yield criterion and thus induces a viscoplastic strain in the region where the rock is over stressed. As discussed in details below, the progressive return of the stress to the yield criterion causes a time-dependent inward displacement of the rock.

The second phase deals with the presence of a rigid casing that prevents further closure of the borehole. In this phase, we are interested in the build-up of the contact pressure at the rock-casing interface, as well as its asymptotic value corresponding to the vanishing of the viscoplastic strain rate. The geometry of the borehole is shown in Fig. 1.

The neighborhood of the borehole, where the stress state violates the yield criterion, is identified as the viscoplastic region $a \leq r \leq b(t)$, where $b(t)$ corresponds to the radius at which the stress state exactly fulfills the yield criterion. The radial stress drop taking place at $t = 0^+$ triggers an elastic inward displacement, and the initial viscoplastic region corresponds to the annulus $a \leq r \leq b(0^+)$, where the elastic stress state violates the yield criterion. The progressive return of the stress state to the yield criterion is accompanied by a viscoplastic deformation that is associated with failure of the rock.

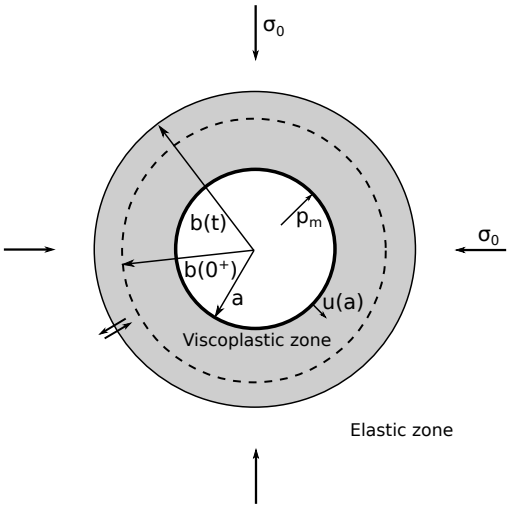

Figure 1: Viscoplastic annulus around the borehole

2.2 Constitutive response

An elasto-viscoplastic constitutive model in the spirit of Perzyna's theory [1966] is adopted to simulate the time-dependent response of soft rocks. It is motivated by the observation that progressive irreversible deformation takes place in laboratory creep test for such rocks. This constitutive model is characterized by a Mohr-Coulomb (M-C) yield criterion $f(\sigma_r, \sigma_\theta)$, a M-C non-associated plastic potential $g(\sigma_r, \sigma_\theta)$, and a Bingham viscoplastic model for the deviatoric response of the rock. Since the principal directions remain fixed in this problem, the constitutive response can directly be expressed in the cylindrical coordinates system. The M-C yield criterion $f(\sigma_r, \sigma_\theta)$ and the M-C plastic potential $g(\sigma_r, \sigma_\theta)$ are defined as

$$f = \sigma_\theta - k\sigma_r - q \quad \sigma_\theta \geq \sigma_r \geq 0 \tag{2}$$

and

$$g = \sigma_\theta - k_f \sigma_r \tag{3}$$

with

$$k = \tan^2\left(\frac{\pi}{4} + \frac{\phi}{2}\right), \quad k_f = \tan^2\left(\frac{\pi}{4} + \frac{\psi}{2}\right),$$

where q, ϕ and ψ are defined as the unconfined compressive strength, the friction angle and the dilation angle, respectively. The yield criterion $f(\sigma_r, \sigma_\theta) = 0$ separates the elastic and the viscoplastic region of the rock in the principal stress space. For $f < 0$, the incremental response of the rock is purely elastic, while for $f > 0$, the strain rate has both an elastic and a viscoplastic component

$$\dot{\epsilon}_{r,\theta} = \dot{\epsilon}^e_{r,\theta} + \dot{\epsilon}^{vp}_{r,\theta}. \tag{4}$$

The strain rate can advantageously be decomposed into a volumetric part $\epsilon = \epsilon_r + \epsilon_\theta$ and a deviatoric part $e_{r,\theta}$ as

$$\dot{\epsilon}_{r,\theta} = \frac{\dot{\epsilon}}{2} + \dot{e}_{r,\theta} \tag{5}$$

with

$$\dot{\epsilon} = \dot{\epsilon}^e + \dot{\epsilon}^{vp}, \quad \dot{e}_{r,\theta} = \dot{e}^e_{r,\theta} + \dot{e}^{vp}_{r,\theta}. \tag{6}$$

The elastic component satisfies Hooke's law

$$2G\dot{e}^e_{r,\theta} = \dot{s}_{r,\theta}, \quad \frac{G}{1-2\nu}\dot{\epsilon}^e = \dot{\sigma}, \tag{7}$$

where

$$\sigma = \frac{\sigma_r + \sigma_\theta}{2} \tag{8}$$

is the in-plane mean stress, and

$$s_{r,\theta} = \sigma_{r,\theta} - \sigma \tag{9}$$

are the deviatoric stress components. The viscoplastic strain rates meanwhile satisfy the non-associated flow rule (3)

$$\dot{\epsilon}_r^{vp} = -\dot{\lambda} k_f, \quad \dot{\epsilon}_\theta^{vp} = \dot{\lambda}, \tag{10}$$

with $\dot{\lambda}$ denoting the viscoplastic strain rate multiplier.

It is convenient to introduce the deviatoric stress invariant $s > 0$ and deviatoric strain invariant $e > 0$ as

$$s = s_\theta = -s_r, \quad e = e_\theta = -e_r. \tag{11}$$

In view of (5) and (11), the viscoplastic strain rate in (10) can be expressed as

$$\dot{\epsilon}_r^{vp} = -\frac{2k_f}{k_f + 1}\dot{e}^{vp}, \quad \dot{\epsilon}_\theta^{vp} = \frac{2}{k_f + 1}\dot{e}^{vp}. \tag{12}$$

The volumetric viscoplastic strain rate deduced from (12)

$$\dot{\epsilon}^{vp} = -\frac{2\,(k_f - 1)}{k_f + 1}\dot{e}^{vp} \tag{13}$$

generally indicates dilation of the rock in the viscoplastic region as $k_f \geq 1$. Fig. 2 shows the decomposition of the viscoplastic strain rate based on (5).

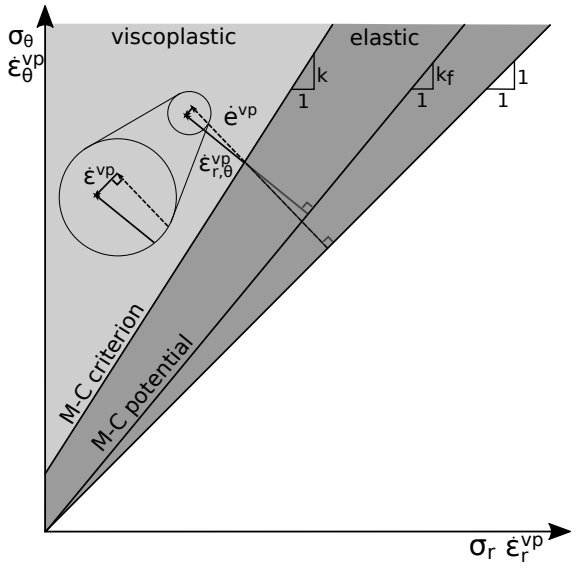

Figure 2: Viscoplastic strain rate decomposition

The deviatoric invariant $\dot{e}^{vp}$ is taken to be proportional to the over-stress invariant Δs as

$$\eta \dot{e}^{vp} = \Delta s, \tag{14}$$

with dynamic viscosity η. The over-stress invariant Δs is defined as

$$\Delta s = s - s_l \tag{15}$$

with s_l denoting the limiting value of the deviatoric stress invariant according to the M-C yield criterion

$$s_l = \frac{k-1}{k+1}\left(\frac{q}{k-1} + \sigma\right). \tag{16}$$

It can readily be shown that Δs is given by (see Fig. 3)

$$\Delta s = \frac{\sigma_\theta - k\sigma_r - q}{k+1}. \tag{17}$$

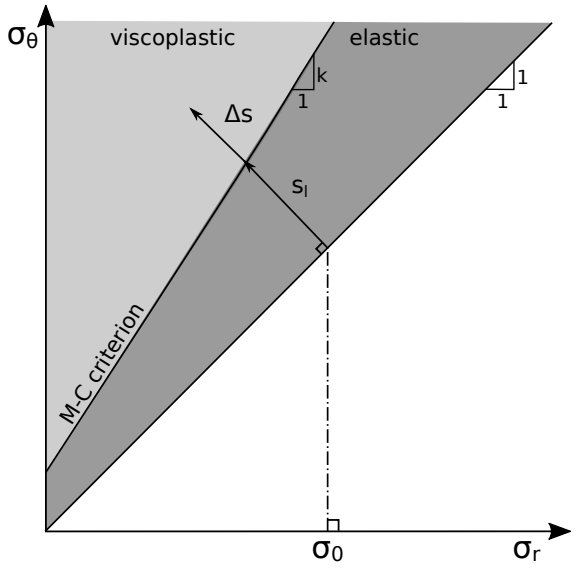

Figure 3: Deviatoric overstress and limiting deviatoric stress

With (12), (14) and (17) the viscoplastic response of the rock is fully determined for the current stress state.

The assumed deviatoric viscoplastic behavior of the soft rock actually corresponds to a Bingham rheological model (Fig. 4). This rheological model consists of a dashpot representing the dynamic viscosity, and a frictional slider representing the M-C yield criterion and the M-C non-associated plastic potential. The viscoplastic behavior is derived from the parallel connection of the dashpot and the slider, which couples the viscosity and the plasticity together. Referring to Fig. 3, while the deviatoric stress invariant s is applied on this model, the dashpot is loaded by the over-stress invariant Δs and the limiting deviatoric stress invariant s_l is transmitted by the slider.

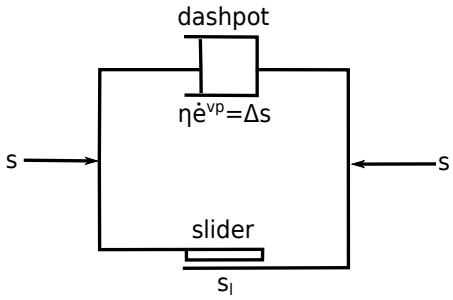

Figure 4: Bingham rheological model

2.3 Field equations

The progressive closure of the borehole is assumed to be a quasi-static process and thus the equilibrium equations are satisfied at all time. Accounting for plane strain and axisymmetric condition, only one equilibrium equation remains

$$\frac{\partial \sigma_r}{\partial r} + \frac{\sigma_r - \sigma_\theta}{r} = 0. \tag{18}$$

On account of no rotation of the principal stress, the rate form of Hooke's law (7) together with $\dot{\epsilon}^e_{r,\theta}$ from (4) can be integrated to yield

$$\sigma_{r,\theta} = \frac{2G}{1-2\nu}\left[(1-\nu)\left(\epsilon_{r,\theta} - \epsilon^{vp}_{r,\theta}\right) + \nu\left(\epsilon_{\theta,r} - \epsilon^{vp}_{\theta,r}\right)\right], \tag{19}$$

where

$$\epsilon^{vp}_{r,\theta} = \int_0^t \dot{\epsilon}^{vp}_{r,\theta} dt. \tag{20}$$

The total strain $\epsilon_{r,\theta}$ is related to the radial displacement u according to

$$\epsilon_r = -\frac{\partial u}{\partial r}, \quad \epsilon_\theta = -\frac{u}{r}. \tag{21}$$

Equation (18)–(21) with the integration of (12) are then combined to yield the governing differential equation for the displacement u

$$-\frac{\partial^2 u}{\partial r^2} - \frac{1}{r}\frac{\partial u}{\partial r} + \frac{u}{r^2} + \alpha_1 \frac{\partial e^{vp}}{\partial r} + \alpha_2 \frac{e^{vp}}{r} = 0. \tag{22}$$

Numbers α_1 and α_2 are defined as

$$\alpha_1 = \frac{2\left(k_f\left(1-\nu\right)-\nu\right)}{\left(1-\nu\right)\left(k_f+1\right)}, \quad \alpha_2 = \frac{2\left(1-2\nu\right)}{1-\nu},$$

with $\alpha_1 \in [0, 1.5]$ and $\alpha_2 \in [0, 2]$ since $\nu \in [0, 0.5]$ and provided that k_f is restricted to the range $[1, 3]$.

2.4 Initial condition, boundary conditions and free boundary condition

The governing equation (22) embeds an integral of the viscoplastic strain rate, itself a function of the stress state. Its solution requires therefore an initial condition besides two boundary conditions. An additional condition is also needed to locate the evolving viscoplastic boundary.

Initial condition. The initial condition corresponds to the elastic state at $t = 0^+$ resulting from the sudden pressure drop at the borehole wall (to mimic the drilling operation). The instantaneous stress field and the displacement field around the borehole is given by the Lamé solution (see, for instance, Fjaer et al. [2008])

$$\sigma_r\left(r, 0^+\right) = \sigma_0 - \left(\sigma_0 - p_m\right)\frac{a^2}{r^2}, \quad \sigma_\theta\left(r, 0^+\right) = \sigma_0 + \left(\sigma_0 - p_m\right)\frac{a^2}{r^2}, \tag{23}$$

$$u\left(r, 0^+\right) = -\frac{\sigma_0 - p_m}{2G}\frac{a^2}{r}. \tag{24}$$

To guarantee that a viscoplastic region develops around the borehole, the stress drop $\sigma_0 - p_m$ must satisfy the condition

$$p_m < \frac{2\sigma_0 - q}{k+1} \tag{25}$$

If (25) is met, the initial viscoplastic boundary is located at $r = b\left(0^+\right)$

$$b\left(0^+\right) = a\sqrt{\frac{(k+1)\left(\sigma_0 - p_m\right)}{q + (k-1)\,\sigma_0}}. \tag{26}$$

In other words, the elastic stress field (23) violates the M-C criterion in the annulus $a < r < b(0^+)$.

Boundary condition at $r = a$. The nature of the boundary condition at $r = a$ depends on whether there is a rock-casing contact or not. After the initial radial stress drop at $t = 0^+$, the radial stress at the borehole is assumed to be constant until $t = t_c$, when the rock enters into contact with the casing

$$\dot{\sigma}_r\left(a, t\right) = 0 \quad 0^+ \leq t \leq t_c. \tag{27}$$

For $t \geq t_c$, further closure of the borehole is prevented by the rigid casing. Hence

$$\dot{u}\left(a, t\right) = 0 \quad t \geq t_c. \tag{28}$$

The contact time t_c is determined by the contact condition $u\left(a, t_c\right) = a_c - a$, where $u\left(a, t_c\right)$ is computed based on the boundary condition (27) and a_c denotes the outer radius of the casing.

Boundary condition at $r = b\left(t\right)$. Formulation of the boundary condition at the evolving viscoplastic boundary $r = b\left(t\right)$ first requires the definition of two different time derivatives at $r = b\left(t\right)$:

1. Type I time derivative, denoted by $\dot{(\ )}$, is calculated at the fixed radius r at the moment when the viscoplastic boundary is at r, i.e., it is the rate of change perceived by an observer located at r, when $b(t) = r$.

2. Type II time derivative, denoted by $\frac{\partial(\ )}{\partial t}$, is evaluated on the evolving viscoplastic boundary, i.e., it is the rate of change viewed by an observer sitting on $b(t)$.

These two time derivatives at $r = b(t)$ are connected by the chain rule

$$\frac{\partial(\ )}{\partial t} = \dot{(\ )} + \frac{\partial(\ )}{\partial r}\dot{b}. \tag{29}$$

The M-C yield criterion (2) must be satisfied on the evolving viscoplastic boundary, i.e., $f\left(\sigma_r^b, \sigma_\theta^b\right) = 0$, where $\sigma_{r,\theta}^b(t) = \sigma_{r,\theta}(b(t), t)$, so the corresponding rate form must be fulfilled also

$$\frac{\partial \sigma_\theta^b}{\partial t} - k\frac{\partial \sigma_r^b}{\partial t} = 0. \tag{30}$$

At $r = b(t)$, $\dot{\epsilon}_r^{vp} = \dot{\epsilon}_\theta^{vp} = 0$; hence, the two principal stress rates $\dot{\sigma}_r^b$ and $\dot{\sigma}_\theta^b$ must satisfy the Lamé solution expressed in rate form, i.e.,

$$\dot{\sigma}_r^b + \dot{\sigma}_\theta^b = 0. \tag{31}$$

Equation (30) and (31) depict the nature of the stress change at $r = b(t)$ from the point of view of two different observers. Combining (29)–(31) yields

$$\dot{\sigma}_r^b = \left(\frac{\partial \sigma_\theta^b}{\partial r} - k\frac{\partial \sigma_r^b}{\partial r}\right)\frac{\dot{b}}{(k+1)} \tag{32}$$

and

$$\frac{\partial \sigma_r^b}{\partial t} = \left(\frac{\partial \sigma_r^b}{\partial r} + \frac{\partial \sigma_\theta^b}{\partial r}\right)\frac{\dot{b}}{(k+1)}, \tag{33}$$

where (33) is the general boundary condition on the evolving viscoplastic boundary.

When the viscoplastic region grows, the evolving viscoplastic boundary moves into the elastic region, so the spatial derivative $\frac{\partial(\ )}{\partial r}$ on the expanding viscoplastic boundary can be evaluated analytically on the elastic side from the Lamé solution. The Lamé solution in (23) and (24) is modified by substituting $p_m \to \sigma_r^b$ and $a \to b\,(t)$. Hence,

$$\frac{\partial \sigma_r^b}{\partial r} = \frac{2\left(\sigma_0 - \sigma_r^b\right)}{b}, \quad \frac{\partial \sigma_\theta^b}{\partial r} = -\frac{2\left(\sigma_0 - \sigma_r^b\right)}{b}, \quad \frac{\partial u^b}{\partial r} = \frac{\left(\sigma_0 - \sigma_r^b\right)}{2G}. \tag{34}$$

Substituting (34) into (33) yields the expanding viscoplastic boundary condition

$$\frac{\partial \sigma_r^b}{\partial t} = 0. \tag{35}$$

In view of the chain rule (29), (35) implies that

$$\dot{\sigma}_{r,\theta}^b = -\frac{\partial \sigma_{r,\theta}^b}{\partial r}\dot{b} \quad \text{if} \quad \dot{b} > 0. \tag{36}$$

When the viscoplastic boundary is shrinking, the stress return to the yield criterion indicates unloading, so $\frac{\partial \sigma_{r,\theta}^b}{\partial t} < 0$. Fig. 5 illustrates the difference between the stress rate when the viscoplastic boundary expands or shrinks.

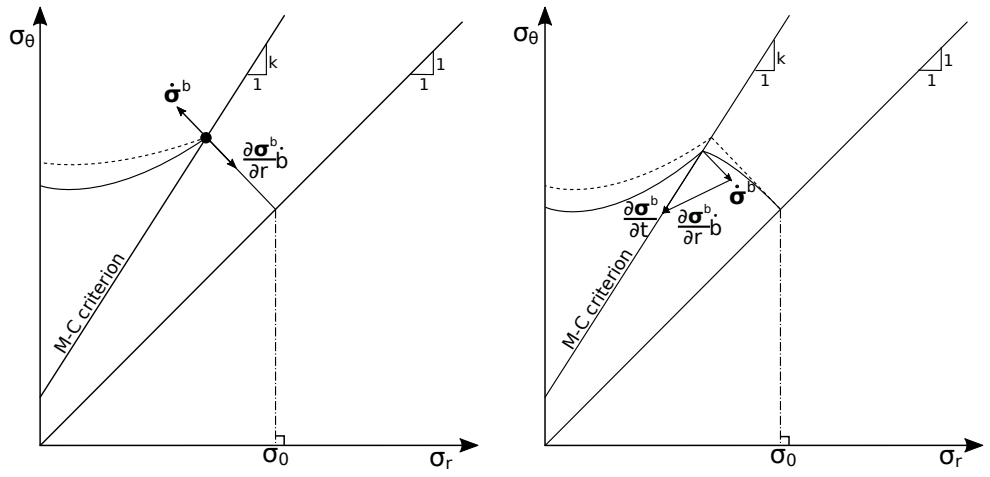

Figure 5: Stress rate and stress gradient on the expanding (left) and shrinking (right) viscoplastic boundary. Left: Dash – previous; Solid – current. Right: Dash – contact; Solid – current.

Free boundary condition. The displacement rate $\dot{u}^b$ at the fixed radius $r = b$ is derived from the Lamé solution expressed in rate form

$$\dot{u}^b = \frac{\dot{\sigma}_r^b}{2G} b. \tag{37}$$

Combined with (29) and (32), the above equation leads to the following expression for $\dot{b}$

$$\dot{b} = \frac{1}{\frac{b}{2G(k+1)}\left(\frac{\partial \sigma_\theta^b}{\partial r} - k\frac{\partial \sigma_r^b}{\partial r}\right) + \frac{\partial u^b}{\partial r}} \frac{\partial u^b}{\partial t}, \tag{38}$$

which represents the free boundary condition. For an expanding viscoplastic boundary $\dot{b} > 0$, (38) can be simplified in view of (34) as

$$\dot{b} = -\frac{2G}{\sigma_0 - \sigma_r^b} \frac{\partial u^b}{\partial t} \tag{39}$$

where $\frac{\partial u^b}{\partial t} < 0$.

In the first phase (before contact), the expansion of the viscoplastic annulus is due to

the monotonic loading of the elastic region caused by the continued reduction of the overstress in the viscoplastic annulus (Fig. 6 – upper). In the second phase (after contact), the contact pressure build-up results in the shrinkage of the viscoplastic annulus (Fig. 6 – lower).

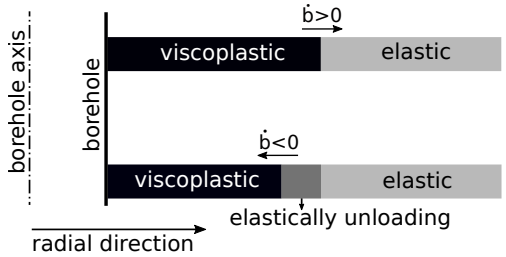

Figure 6: Changing viscoplastic and elastic domain before (upper) and after (lower) contact

3 Scaling

Section 2 formulated a closed mathematical model that governs the evolution of the stress and displacement field around a borehole following drilling. A dimensionless formulation of this model requires the introduction of stress scale S, displacement scale U, time scale T, and length scale a (the nominal borehole radius)

$$\sigma = S\tilde{\sigma} \quad u = U\tilde{u} \quad t = T\tau \quad r = a\left(\chi\delta + 1\right) \tag{40}$$

with $\tilde{(\ )}$ denoting the dimensionless field variable as function of scaled time τ and scaled coordinate $\chi \in [0, 1]$. The dimensionless thickness of the evolving viscoplastic region $\delta\left(\tau\right)$ is given by

$$\delta = \frac{b}{a} - 1. \tag{41}$$

Scales S, U and T are determined in the process of converting the dimensional mathematical model to the dimensionless one. After introducing the scales, (14) can be written as

$$\dot{\tilde{e}}^{vp} = \mathcal{G}_1 \frac{\tilde{\sigma}_\theta - k\tilde{\sigma}_r}{k+1} - \mathcal{G}_2 \frac{1}{k+1}, \tag{42}$$

and (19) as

$$\tilde{\sigma}_{r,\theta} = \mathcal{G}_3 \left(-\frac{a_{3,4}}{\delta} \frac{\partial \tilde{u}}{\partial \chi} - \frac{a_{4,3}\tilde{u}}{\chi\delta + 1} \right) + \frac{2\mathcal{G}_4}{k_f + 1} \left(k_f a_{3,4} - a_{4,3} \right) \tilde{e}^{vp} \tag{43}$$

with

$$a_3 = \frac{2\left(1-\nu\right)}{1-2\nu} \quad a_4 = \frac{2\nu}{1-2\nu}.$$

The dimensionless groups $\mathcal{G}_1$–$\mathcal{G}_4$ appearing in the above two equations are defined as

$$\mathcal{G}_1 = \frac{ST}{\eta} \quad \mathcal{G}_2 = \frac{Tq}{\eta} \quad \mathcal{G}_3 = \frac{GU}{aS} \quad \mathcal{G}_4 = \frac{G}{S}.$$

Setting $\mathcal{G}_1$, $\mathcal{G}_2$ and $\mathcal{G}_3$ to 1 and redefining $\mathcal{G}_4$ as the dimensionless shear modulus γ leads to

$$S = q \quad T = \frac{\eta}{q} \quad U = \frac{aq}{G} \quad \gamma = \frac{G}{q} \tag{44}$$

where γ is typically of order $O(10^2)$.

After scaling, (22) becomes

$$-\frac{1}{\delta^2}\frac{\partial^2 \tilde{u}}{\partial \chi^2} - \frac{1}{\left(\chi\delta + 1\right)\delta}\frac{\partial \tilde{u}}{\partial \chi} + \frac{\tilde{u}}{\left(\chi\delta + 1\right)^2} + \frac{\alpha_1\gamma}{\delta}\frac{\partial \tilde{e}^{vp}}{\partial \chi} + \frac{\alpha_2\gamma\tilde{e}^{vp}}{1+\chi\delta} = 0, \tag{45}$$

which after differentiation with respect to τ at constant χ reads

$$-\frac{1}{\delta^2}\frac{\partial^3 \tilde{u}}{\partial \chi^2 \partial \tau} - \frac{1}{\left(\chi\delta + 1\right)\delta}\frac{\partial^2 \tilde{u}}{\partial \chi \partial \tau} + \frac{1}{\left(\chi\delta + 1\right)^2}\frac{\partial \tilde{u}}{\partial \tau} + \frac{\alpha_1\gamma}{\delta}\frac{\partial^2 \tilde{e}^{vp}}{\partial \chi \partial \tau} + \frac{\alpha_2\gamma}{1+\chi\delta}\frac{\partial \tilde{e}^{vp}}{\partial \tau} + A\dot{\delta} = 0 \tag{46}$$

with

$$A = \frac{2}{\delta^3}\frac{\partial^2 \tilde{u}}{\partial \chi^2} + \frac{1}{(\chi\delta+1)\,\delta}\left(\frac{\chi}{\chi\delta+1}+\frac{1}{\delta}\right)\frac{\partial \tilde{u}}{\partial \chi} - \frac{2\chi\tilde{u}}{(1+\chi\delta)^3} - \frac{\alpha_1\gamma}{\delta^2}\frac{\partial \tilde{e}^{vp}}{\partial \chi} - \frac{\alpha_2\gamma\chi\tilde{e}^{vp}}{(1+\chi\delta)^2},$$

and the differentiation of (43) yields

$$\frac{\partial \tilde{\sigma}_{r,\theta}}{\partial \tau} = -\frac{\alpha_{3,4}}{\delta}\frac{\partial^2 \tilde{u}}{\partial \chi \partial \tau} - \frac{\alpha_{4,3}}{\chi\delta+1}\frac{\partial \tilde{u}}{\partial \tau} + \frac{2\gamma\left(k_f\alpha_{3,4}-\alpha_{4,3}\right)}{k_f+1}\frac{\partial \tilde{e}^{vp}}{\partial \tau} + \left(\frac{\alpha_{3,4}}{\delta^2}\frac{\partial \tilde{u}}{\partial \chi} + \frac{\alpha_{4,3}\chi\tilde{u}}{(\chi\delta+1)^2}\right)\dot{\delta}. \tag{47}$$

The viscoplastic strain rate $\frac{\partial \tilde{e}^{vp}}{\partial \tau}$ is however unknown in (46) and (47). With the chain rule

$$\frac{\partial(\ )}{\partial \tau} = (\dot{\ }) + \frac{\chi}{\delta}\frac{\partial(\ )}{\partial \chi}\dot{\delta}, \tag{48}$$

$\frac{\partial \tilde{e}^{vp}}{\partial \tau}$ can be expressed as the sum of $\dot{\tilde{e}}^{vp}$, a known function of the current stress, and an advective term $\frac{\chi}{\delta}\frac{\partial \tilde{e}^{vp}}{\partial \chi}\dot{\delta}$ due to the mapping from the viscoplastic annulus to the unit plane. Hence,

$$\frac{\partial \tilde{e}^{vp}}{\partial \tau} = \dot{\tilde{e}}^{vp} + \frac{\chi}{\delta}\frac{\partial \tilde{e}^{vp}}{\partial \chi}\dot{\delta}, \tag{49}$$

$$\frac{\partial^2 \tilde{e}^{vp}}{\partial \chi \partial \tau} = \frac{\partial \dot{\tilde{e}}^{vp}}{\partial \chi} + \frac{1}{\delta}\left(\chi\frac{\partial^2 \tilde{e}^{vp}}{\partial \chi^2} + \frac{\partial \tilde{e}^{vp}}{\partial \chi}\right)\dot{\delta}. \tag{50}$$

(49) and (50) can be substituted into (46) and (47) to yield

$$-\frac{1}{\delta^2}\frac{\partial^3 \tilde{u}}{\partial \chi^2 \partial \tau} - \frac{1}{(\chi\delta+1)\,\delta}\frac{\partial^2 \tilde{u}}{\partial \chi \partial \tau} + \frac{1}{(\chi\delta+1)^2}\frac{\partial \tilde{u}}{\partial \tau} + \frac{\alpha_1\gamma}{\delta}\frac{\partial \dot{\tilde{e}}^{vp}}{\partial \chi} + \frac{\alpha_2\gamma\dot{\tilde{e}}^{vp}}{\chi\delta+1} + B\dot{\delta} = 0 \tag{51}$$

with

$$B = \frac{2}{\delta^3}\frac{\partial^2 \tilde{u}}{\partial \chi^2} + \frac{1}{(\chi\delta+1)\,\delta}\left(\frac{\chi}{\chi\delta+1} + \frac{1}{\delta}\right)\frac{\partial \tilde{u}}{\partial \chi} - \frac{2\chi\tilde{u}}{(\chi\delta+1)^3} + \frac{\alpha_1\gamma\chi}{\delta^2}\frac{\partial^2 \tilde{e}^{vp}}{\partial \chi^2} + \frac{\alpha_2\gamma\chi}{(\chi\delta+1)\,\delta}\frac{\partial \tilde{e}^{vp}}{\partial \chi} - \frac{\alpha_2\gamma\chi\tilde{e}^{vp}}{(\chi\delta+1)^2},$$

and

$$\frac{\partial \tilde{\sigma}_{r,\theta}}{\partial \tau} = -\frac{\alpha_{3,4}}{\delta}\frac{\partial^2 \tilde{u}}{\partial \chi \partial \tau} - \frac{\alpha_{4,3}}{\chi\delta+1}\frac{\partial \tilde{u}}{\partial \tau} + \frac{2\gamma\left(k_f\alpha_{3,4} - \alpha_{4,3}\right)}{k_f+1}\dot{\tilde{e}}^{vp} + \left(\frac{\alpha_{3,4}}{\delta^2}\frac{\partial \tilde{u}}{\partial \chi} + \frac{\alpha_{4,3}\chi\tilde{u}}{(\chi\delta+1)^2} + \frac{2\gamma\left(k_f\alpha_{3,4} - \alpha_{4,3}\right)\chi}{(k_f+1)\,\delta}\frac{\partial \tilde{e}^{vp}}{\partial \chi}\right)\dot{\delta}. \quad (52)$$

Based on Section 2.4, the initial condition, the boundary conditions and the free boundary condition after scaling are given below.

Initial condition.

$$\tilde{\sigma}_r\left(\chi, 0^+\right) = \tilde{\sigma}_0 - \frac{\tilde{\sigma}_0 - \tilde{p}_m}{\left(\chi\delta\left(0^+\right)+1\right)^2}, \quad \tilde{\sigma}_\theta\left(\chi, 0^+\right) = \tilde{\sigma}_0 + \frac{\tilde{\sigma}_0 - \tilde{p}_m}{\left(\chi\delta\left(0^+\right)+1\right)^2}, \quad (53)$$

$$\tilde{u}\left(\chi, 0^+\right) = -\frac{\tilde{\sigma}_0 - \tilde{p}_m}{2}\frac{1}{\chi\delta\left(0^+\right)+1}. \quad (54)$$

with $\delta\left(0^+\right)$ given by

$$\delta\left(0^+\right) = \sqrt{\frac{(k+1)(\tilde{\sigma}_0 - \tilde{p}_m)}{(k-1)\tilde{\sigma}_0 + 1}} - 1 \quad (55)$$

Boundary condition at $\chi = 0$.

$$\frac{\partial \tilde{\sigma}_r\left(0, \tau\right)}{\partial \tau} = 0 \quad 0^+ \leq \tau \leq \tau_c, \quad (56)$$

with

$$\tilde{u}\left(0,\tau_c\right) = -\omega \tag{57}$$

and

$$\frac{\partial \tilde{u}\left(0,\tau\right)}{\partial \tau} = 0 \quad \tau \geq \tau_c. \tag{58}$$

Boundary condition (57) introduces another number, the dimensionless gap ω, defined as

$$\omega = \frac{(a-a_c)G}{aq}$$

Boundary condition at $\chi = 1$.

$$\frac{\partial \tilde{\sigma}_r}{\partial \tau} = \left(\frac{\partial \tilde{\sigma}_r}{\partial \chi} + \frac{\partial \tilde{\sigma}_\theta}{\partial \chi}\right)\frac{\dot{\delta}}{(k+1)\,\delta}, \qquad \chi = 1,\, \tau > 0, \tag{59}$$

$$\frac{\partial \tilde{\sigma}_\theta}{\partial \tau} - k\frac{\partial \tilde{\sigma}_r}{\partial \tau} = 0 \qquad \chi = 1,\, \tau > 0, \tag{60}$$

with the special form of (59) before the rock-casing contact

$$\frac{\partial \tilde{\sigma}_r}{\partial \tau} = 0, \qquad \chi = 1,\, 0 < \tau \leq \tau_c. \tag{61}$$

Free boundary condition.

$$\dot{\delta} = \frac{1}{\frac{\delta+1}{2(k+1)\delta}\left(\frac{\partial \tilde{\sigma}_\theta}{\partial \chi} - k\frac{\partial \tilde{\sigma}_r}{\partial \chi}\right) + \frac{1}{\delta}\frac{\partial \tilde{u}}{\partial \chi}}\frac{\partial \tilde{u}}{\partial \tau}, \qquad \chi = 1,\, \tau > 0, \tag{62}$$

with the special form of (62) before the rock-casing contact

$$\dot{\delta} = -\frac{2\,(k+1)}{(k-1)\,\tilde{\sigma}_0 + 1}\frac{\partial \tilde{u}}{\partial \tau}, \qquad \chi = 1,\, 0 < \tau \leq \tau_c. \tag{63}$$

In summary, the mathematical model yields a solution $\mathbb{S} = \{\tilde{u}, \tilde{\sigma}_{r,\theta}, \tilde{e}^{vp}, \delta, \tau_c\}$ of the form

$$\mathbb{S} = \mathbb{S}\left(\chi, \tau; \gamma, \nu, k, k_f, \tilde{\sigma}_0, \tilde{p}_m, \omega\right) \tag{64}$$

4 Numerical scheme

The partial differential equations (51) and (52) are semi-discretized on space by replacing the spatial derivatives $\frac{\partial^2(\ )}{\partial\chi^2}$ and $\frac{\partial(\ )}{\partial\chi}$ with finite differences. The interval $\chi \in [0, 1]$ is discretized into a set of equidistant nodes χ_i, $i = 0 \cdots n$, with constant spacing $\Delta\chi = \frac{1}{n}$, so that

$$\chi_0 = 0 \quad \cdots \quad \chi_i = i\Delta\chi \quad \cdots \quad \chi_n = 1, \tag{65}$$

where χ_0 and χ_n are located at the borehole and the evolving viscoplastic boundary, respectively. The subscript $(\ )_i$ denotes the field variable at χ_i. The finite difference schemes used to solve phase 1 and 2 differ slightly, to account for the different boundary condition at $\chi = 0$ before and after the casing/rock contact.

Before the rock-casing contact. The spatial derivatives of the displacement at χ_i, $i = 0 \cdots n$, are evaluated with the central difference scheme

$$\left.\frac{\partial^2\tilde{u}}{\partial\chi\partial\tau}\right|_{\chi=\chi_i} \simeq \frac{1}{2\Delta\chi}\left(\frac{d\tilde{u}_{i+1}}{d\tau} - \frac{d\tilde{u}_{i-1}}{d\tau}\right), \quad \left.\frac{\partial^3\tilde{u}}{\partial\chi^2\partial\tau}\right|_{\chi=\chi_i} = \frac{1}{\Delta\chi^2}\left(\frac{d\tilde{u}_{i+1}}{d\tau} - 2\frac{d\tilde{u}_i}{d\tau} + \frac{d\tilde{u}_{i-1}}{d\tau}\right). \tag{66}$$

The Neumann boundary conditions (56) at $\chi = 0$ and (59) at $\chi = 1$ are applied via the introduction of two ghost nodes at $\chi_{-1} = -\Delta\chi$ and at $\chi_{n+1} = 1 + \Delta\chi$. When applying (66) on (51) and (52) at χ_0 and χ_n, $\frac{d\tilde{u}_{-1}}{d\tau}$ and $\frac{d\tilde{u}_{n+1}}{d\tau}$, the displacement rates at the ghost nodes, are calculated using the stress boundary condition at $\chi = 0$ and χ =1. Combining

Hooke's law for $\frac{\partial \tilde{\sigma}_\tau}{\partial \tau}$ (52) with the spatial difference (66), enables to express $\frac{d\tilde{u}_{-1}}{d\tau}$ as

$$\frac{d\tilde{u}_{-1}}{d\tau} = \frac{2\alpha_4 \delta \Delta\chi}{\alpha_3} \frac{d\tilde{u}_0}{d\tau} + \frac{d\tilde{u}_1}{d\tau} + \mathcal{F}\left(\dot{\tilde{e}}^{vp}, \dot{\delta}\right), \tag{67}$$

where the boundary condition (56) has been applied. Substituting (67) back to (51) with the difference scheme (66) finally removes the ghost node term $\frac{d\tilde{u}_{-1}}{d\tau}$. At the evolving boundary, a similar approach is adopted.

The other spatial derivatives are evaluated based on a local interpolation of the field based on Lagrangian polynomials

$$\begin{cases} \frac{\partial(\ )_0}{\partial\chi} = \frac{1}{\Delta\chi}\left(-\frac{1}{2}(\ )_2 + 2(\ )_1 - \frac{3}{2}(\ )_0\right) \\ \frac{\partial(\ )_1}{\partial\chi} = \frac{1}{\Delta\chi}\left(\frac{1}{12}(\ )_4 - \frac{1}{2}(\ )_3 + \frac{3}{2}(\ )_2 - \frac{5}{6}(\ )_1 - \frac{1}{4}(\ )_0\right) \\ \frac{\partial(\ )_i}{\partial\chi} = \frac{1}{\Delta\chi}\left(-\frac{1}{12}(\ )_{i+2} + \frac{2}{3}(\ )_{i+1} - \frac{2}{3}(\ )_{i-1} + \frac{1}{12}(\ )_{i-2}\right) \qquad i = 2\cdots n-2\,, \\ \frac{\partial(\ )_{n-1}}{\partial\chi} = \frac{1}{\Delta\chi}\left(\frac{1}{4}(\ )_n + \frac{5}{6}(\ )_{n-1} - \frac{3}{2}(\ )_{n-2} + \frac{1}{2}(\ )_{n-3} - \frac{1}{12}(\ )_{n-4}\right) \\ \frac{\partial(\ )_n}{\partial\chi} = \frac{1}{\Delta\chi}\left(\frac{3}{2}(\ )_n - 2(\ )_{n-1} + \frac{1}{2}(\ )_{n-2}\right) \end{cases} \tag{68}$$

$$\begin{cases} \frac{\partial^2(\ )_0}{\partial\chi^2} = \frac{1}{\Delta\chi^2}\left(-(\ )_3 + 4(\ )_2 - 5(\ )_1 + 2(\ )_0\right) \\ \frac{\partial^2(\ )_1}{\partial\chi^2} = \frac{1}{\Delta\chi^2}\left(-\frac{1}{12}(\ )_4 + \frac{1}{3}(\ )_3 + \frac{1}{2}(\ )_2 - \frac{5}{3}(\ )_1 + \frac{11}{12}(\ )_0\right) \\ \frac{\partial^2(\ )_i}{\partial\chi^2} = \frac{1}{\Delta\chi^2}\left(-\frac{1}{12}(\ )_{i+2} + \frac{4}{3}(\ )_{i+1} - \frac{5}{2}(\ )_i + \frac{4}{3}(\ )_{i-1} - \frac{1}{12}(\ )_{i-2}\right) \qquad i = 2\cdots n-2\,. \\ \frac{\partial^2(\ )_{n-1}}{\partial\chi^2} = \frac{1}{\Delta\chi^2}\left(\frac{11}{12}(\ )_n - \frac{5}{3}(\ )_{n-1} + \frac{1}{2}(\ )_{n-2} + \frac{1}{3}(\ )_{n-3} - \frac{1}{12}(\ )_{n-4}\right) \\ \frac{\partial^2(\ )_n}{\partial\chi^2} = \frac{1}{\Delta\chi^2}\left(2(\ )_n - 5(\ )_{n-1} + 4(\ )_{n-2} - (\ )_{n-3}\right) \end{cases} \tag{69}$$

After the rock-casing contact. As before the contact, a similar approach is adopted to remove $\frac{d\tilde{u}_{n+1}}{d\tau}$ at χ_n. However, at the borehole, the Dirichlet boundary condition (58) can be applied directly so removing $\frac{d\tilde{u}_{-1}}{d\tau}$ is avoided. The spatial derivative at the borehole can be evaluated based on the Lagrange polynomial as

$$\left.\frac{\partial^2\tilde{u}}{\partial\chi\partial\tau}\right|_{\chi=\chi_0} \simeq \frac{1}{\Delta\chi}\left(\frac{d\tilde{u}_1}{d\tau}-\frac{d\tilde{u}_0}{d\tau}\right), \quad \left.\frac{\partial^3\tilde{u}}{\partial\chi^2\partial\tau}\right|_{\chi=\chi_0} = \frac{1}{\Delta\chi^2}\left(\frac{d\tilde{u}_2}{d\tau}-2\frac{d\tilde{u}_1}{d\tau}+\frac{d\tilde{u}_0}{d\tau}\right). \quad (70)$$

For the other spatial derivatives on the boundary, the corresponding scheme in (68) and (69) are still valid.

State-space method. The state-space method can be applied to any mathematical model which can be described by first order differential equations for each of the state variables. Let $\boldsymbol{y}$ denote the vector of state variables, which here corresponds to the displacement, radial and tangential stress, viscoplastic strain at the nodes of the mesh and to the thickness of the viscoplastic annulus

$$\boldsymbol{y} = (\cdots\ \tilde{u}_i\ \cdots\ \tilde{\sigma}_{r,i}\ \cdots\ \tilde{\sigma}_{\theta,i}\ \cdots\ \tilde{e}_i^{vp}\ \cdots\ \delta)^T \quad i = 0\cdots n. \quad (71)$$

The dimension of the state space variables is thus $(4n+5)\times 1$. The system of the first order differential equations is obtained by replacing the spatial derivatives by the difference schemes (66)–(70) into governing equations (51), (52), (49), at each node χ_i, as well as in the free boundary condition (62). The system of equations can be written in a compact form as

$$\boldsymbol{M}(y)\,\frac{\partial\boldsymbol{y}}{\partial\tau} = \boldsymbol{b}(y), \quad (72)$$

where $\boldsymbol{M}$ is a $(4n+5)\times(4n+5)$ matrix of coefficients and $\boldsymbol{b}$ is a $(4n+5)\times 1$ vector. This system of first order ODE is integrated from the initial conditions at $\tau = 0^+$ using the MATLAB function ODE45.

5 Simulation

5.1 Benchmark simulation

In this section we show results of simulations conducted with the numerical algorithm described in Section 4. Two cases are considered. For the first case, the borehole pressure is kept constant following sudden unloading, so that the borehole deformation remains uninhibited until it reaches a limit state. The objective of this simulation is to verify that the long-term asymptotic solution is indeed in agreement with the classic elastoplastic solution for a constant borehole pressure. For the second case, the borehole closure cannot exceed a threshold corresponding to the placement of a rigid casing and the simulation proceeds until the pressure at the casing/rock interface stabilizes. An alternative to this simulation is also considered. It involves computing the borehole pressure required to maintain the elastoplastic interface at the same position, once the closure reaches the threshold set for the previous simulation. In this alternative, there is further but very limited displacement at the borehole wall.

The initial solution following unloading of the borehole is given by Lamé solution (53)–(55), while the large time asymptotic solution for the case of constant borehole pressure $\tilde{p}_m$ corresponds to the classical elastoplastic solution [Detournay, 1986, Fjaer et al., 2008]

$$\tilde{\sigma}_{rp} = -\tilde{\sigma}_0 + \frac{\tilde{s}_l^0}{k-1}\left(k+1-2\rho^{k-1}\right), \tag{73}$$

$$\tilde{\sigma}_{\theta p} = -\tilde{\sigma}_0 + \frac{\tilde{s}_l^0}{k-1}\left(k+1-2k\rho^{k-1}\right), \tag{74}$$

$$\tilde{u}_p = -\tfrac{1}{2}\tilde{s}_l^0(1+\delta_p)\rho\left[1+\frac{\lambda^\star+2k+2k_f}{(k_f+1)\,(k+k_f)}\left(\rho^{-(k_f+1)}-1\right)+\frac{\lambda^\star}{(k-1)\,(k+k_f)}\left(\rho^{k-1}-1\right)\right], \tag{75}$$

$$\delta_p = \left(\frac{\tilde{\sigma}_0+\dfrac{1}{k-1}}{\dfrac{2}{k+1}\,\tilde{p}_m+\dfrac{1}{k-1}}\right)^{\dfrac{1}{k-1}} - 1, \tag{76}$$

with

$$\rho = \frac{1+\chi\delta_p}{1+\delta_p}; \quad 0 \le \chi \le 1,$$

$$\tilde{s}_l^0 = \frac{k-1}{k+1}\left(\frac{1}{k-1}+\tilde{\sigma}_0\right),$$

$$\lambda^\star = (k-1)\,(k_f-1)+(1-2\nu)\,(k+1)\,(k_f+1)\,.$$

The values of the physical parameters on which the simulations are based are: $a = 0.05$ m, $a_c = 0.045$ m, $G = 0.37$ GPa, $\nu = 0.35$, $q = 6$ MPa, $\phi = 30^\circ$, $\psi = 11.6^\circ$, $\sigma_0 = 30$ MPa, and $p_m = 0$. The rock viscosity is left as an open parameter, as it only affects the time scale defined as $T = \eta/q$ in (44). The corresponding numbers controlling the scaled solution are thus given by $\omega = 6.17$, $\gamma = 61.7$, $k = 3$, $k_f = 1.5$, $\tilde{\sigma}_0 = 5$, $\tilde{p}_m = 0$, $\nu = 0.35$.

The calculations were conducted using 400 nodes in the computational mesh. This number, which was selected on the basis of a convergence study summarized in Appendix, ensures a relative error of about 10^{-4} or less.

Case 1. Fig. 7 shows several isochrones of the stress trajectory in the principal stress space. The progressively reduced stress state evolves from the elastic (Lamé) solution at $\tau = 0^+$ to the plastic solution at $\tau = \infty$. Fig. 8 shows the same results but plots the isochrones of the stress trajectory in the unit plane.

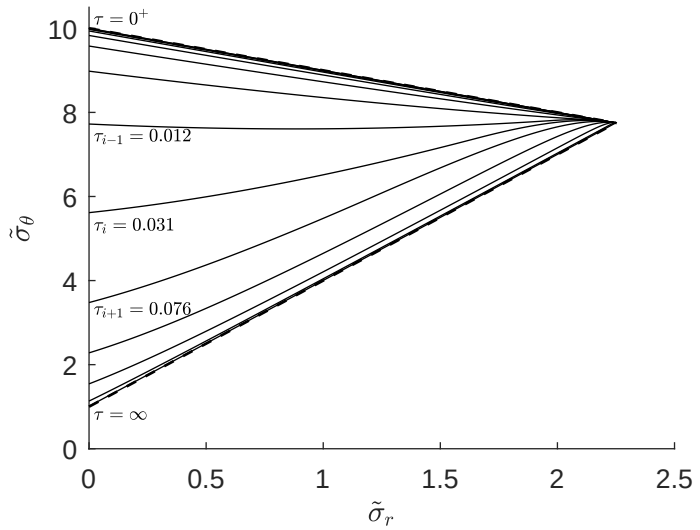

Figure 7: Case 1: Stress state in principal stress space. Upper dash – initial elastic solution; Lower dash – asymptotic plastic solution. The time ratio between each line is $\tau_i/\tau_{i-1} = 2.5$.

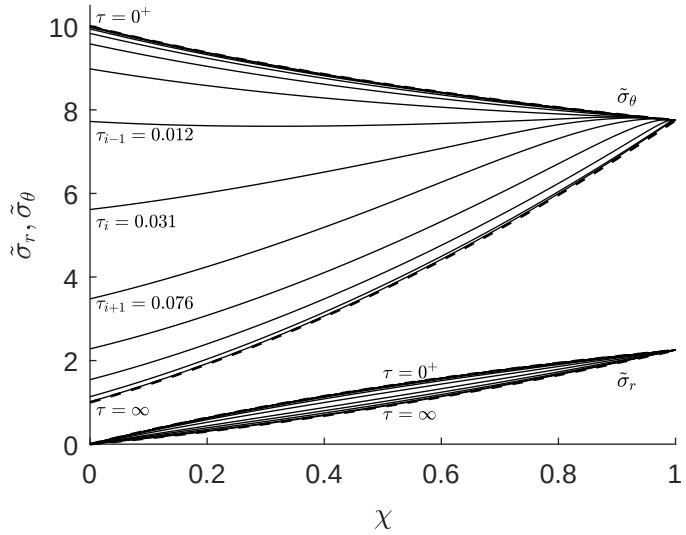

Figure 8: Case 1: Radial stress (lower part) and tangential stress (upper part) in the unit plane. In each part: Upper dash – initial elastic solution; Lower dash – asymptotic plastic solution.

Isochrones of the radial displacement field in the viscoplastic annulus are plotted in Fig. 9. It can be observed that the displacement evolves from the elastic (Lamé) solution to the plastic solution. Evolution of the displacement at the borehole wall and growth of the thickness of the viscoplastic annulus are plotted in Fig. 10. For the set of parameters selected in this numerical simulation, the asymptotic solution is approximately reached at $\tau = 2$, i.e., twice the time scale T in real time. The viscoplastic solution, $\tilde{u}(0, \tau)$ and $\delta(\tau)$ is seen to converge towards the elastoplastic solution $\tilde{u}_p(0)$ and δ_p shown as dashed lines in Fig. 10.

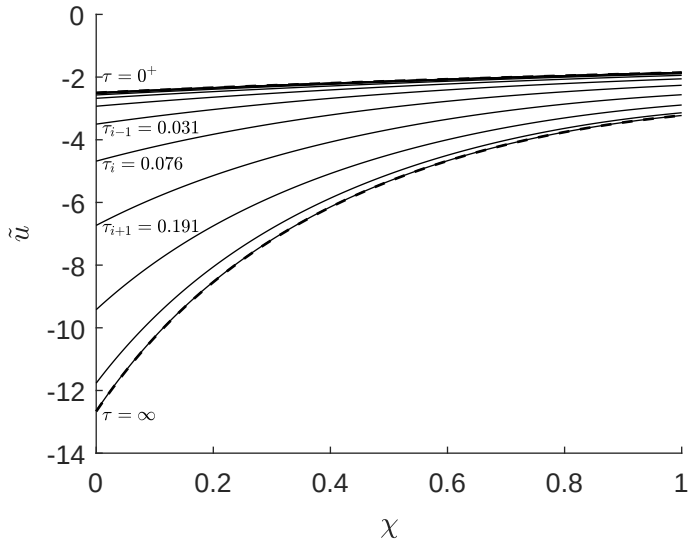

Figure 9: Case 1: Displacement in the unit plane. Upper dash – initial elastic solution; Lower dash – asymptotic plastic solution.

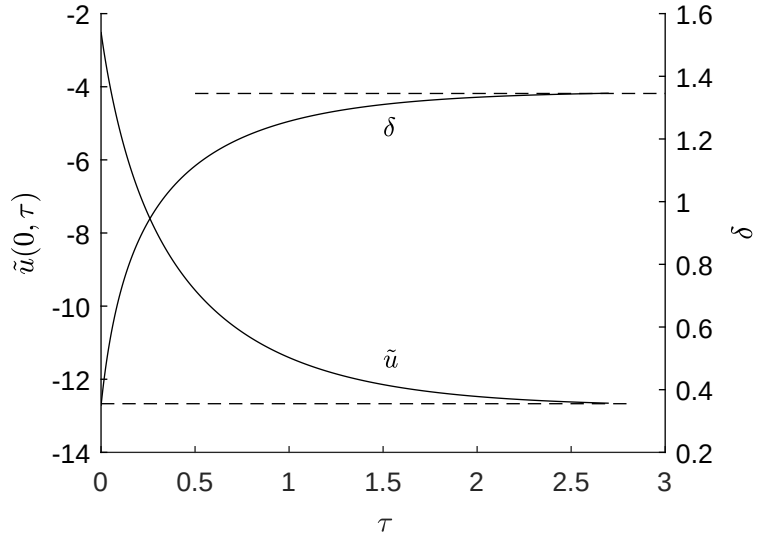

Figure 10: Case 1: Gradually converged borehole displacement and evolving thickness of the viscoplastic boundary. Dash – asymptotic solution.

Case 2. Here the borehole closure is restricted by a rigid casing, i.e. $\tilde{u}^b + \omega \geq 0$. Results of the simulations are illustrated in Figs. 11–13, following the same format as for Case

1, but with the post-contact results shown in gray. Fig. 13 indicates that there is no visible change to the displacement field in the viscoplastic annulus, once contact has taken place, even though the stress continues to evolve until the limit state is reached as can be observed in Figs. 11 and 12.

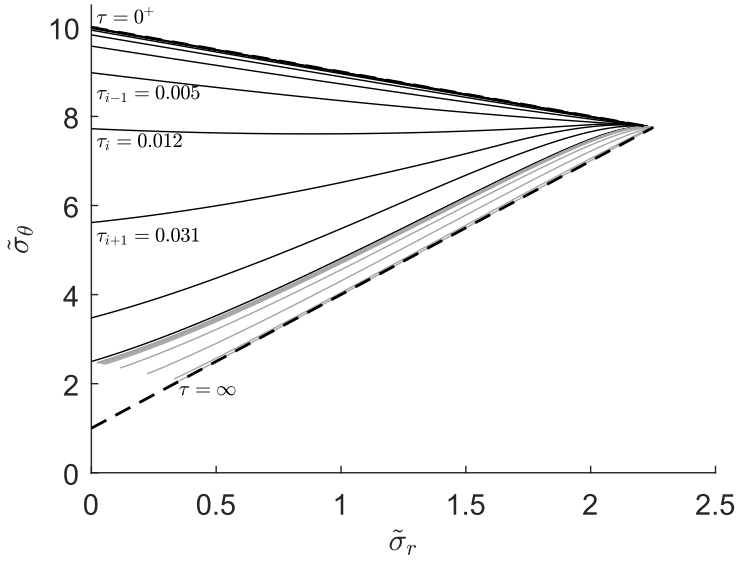

Figure 11: Case 2: Stress state in principal stress space. Black – before contact; Gray – after contact; Upper dash – initial elastic solution; Lower dash – asymptotic plastic solution. The time ratio between each line is $\tau_i/\tau_{i-1} = 2.5$.

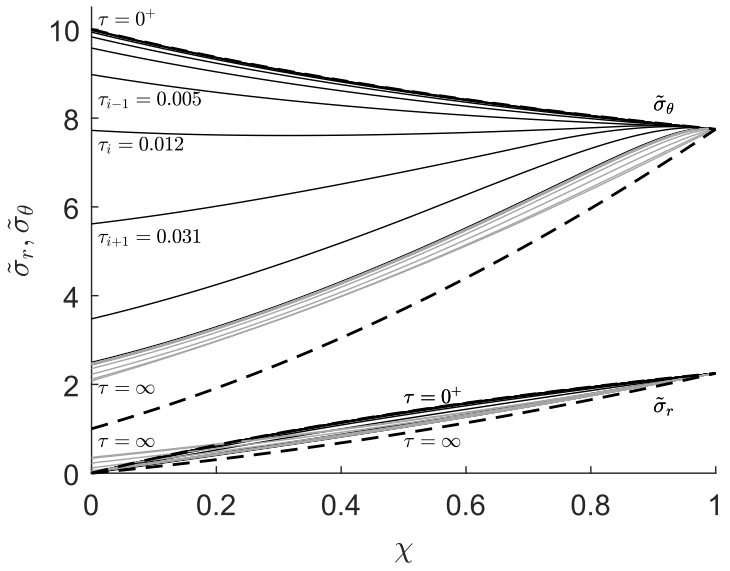

Figure 12: Case 2: Radial stress and tangential stress in the unit plane. Black – before contact; Gray – after contact. In each part: Upper dash – initial elastic solution; Lower dash – asymptotic plastic solution.

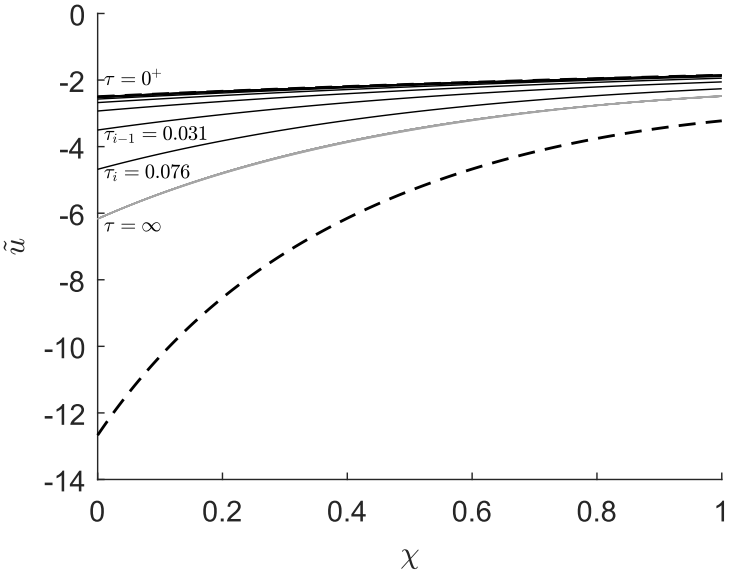

Figure 13: Case 2: Displacement in the unit plane. Black – before contact; Gray – after contact; Upper dash – initial elastic solution; Lower dash – asymptotic plastic solution.

Comparison. Figures 14–16 compare the evolution of the viscoplastic annulus, borehole closure, and interface pressure for Case 1 and 2 and a third simulation where the condition $\dot{\delta} = 0$ is arbitrarily imposed for $\tau > \tau_c$ with τ_c defining the time at which $\tilde{u}(0, \tau_c) + \omega = 0$. For the latter simulation, all the convective terms in the system of ODE (72) vanish since $\dot{\delta} = 0$, thus leading to a simpler form of the equations. Fig. 14 shows that the motion of the viscoplastic boundary is reversed after contact, thus causing some elastic unloading. However, the shrinking of the viscoplastic annulus is quite limited. Plots of $\tilde{u}(0, \tau)$ and $\tilde{\sigma}_r(0, \tau)$ in Figs. 15 and 16 show that the rigid casing solution and the $\dot{\delta} = 0$ solution are relatively close.

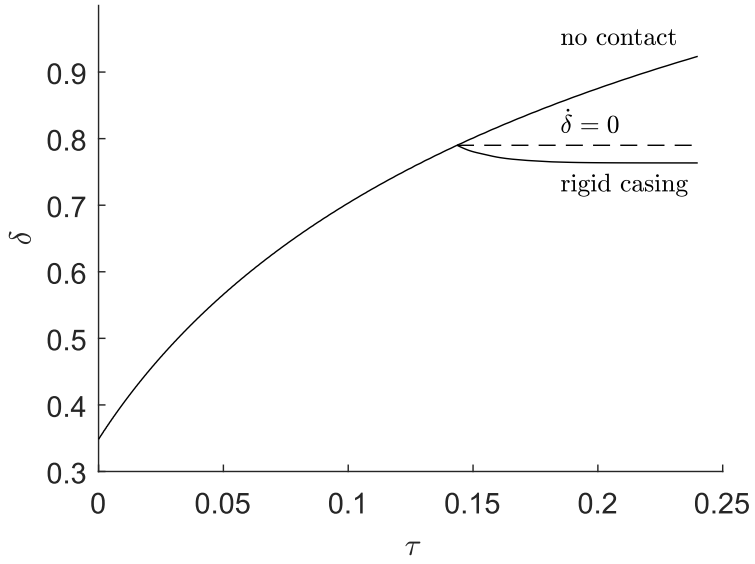

Figure 14: Evolution of viscoplastic annulus for the three simulations

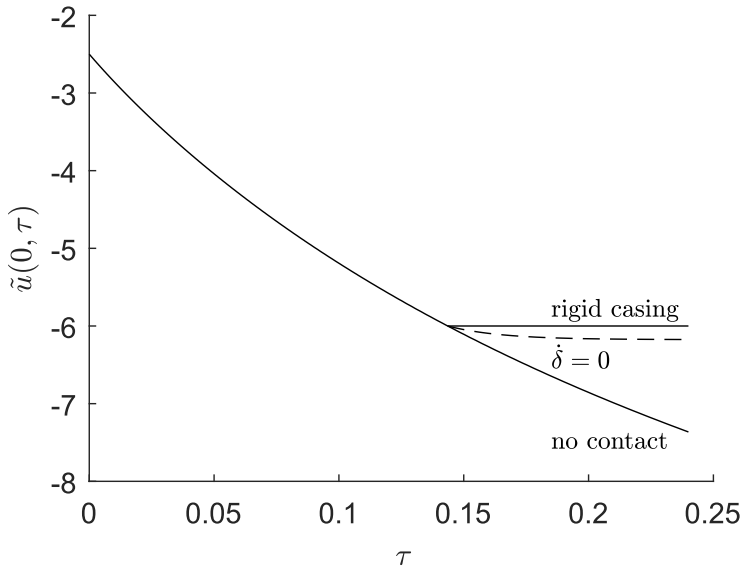

Figure 15: Evolution of the displacement at the borehole for the three simulations.

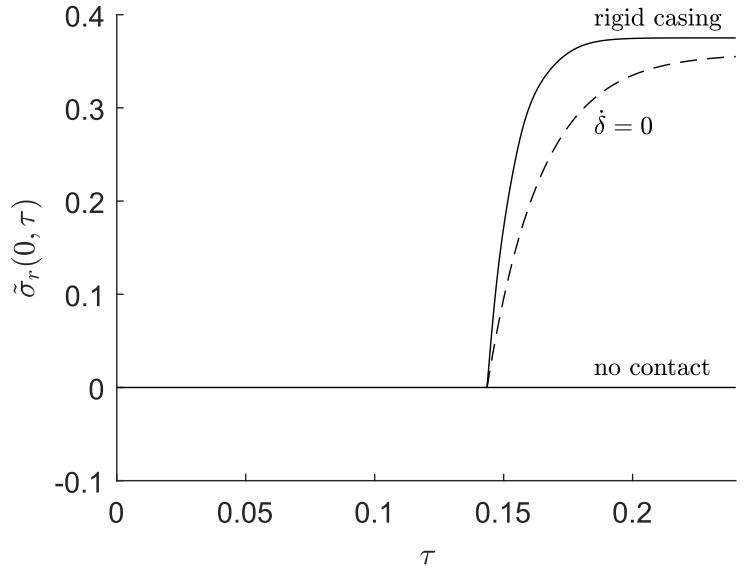

Figure 16: Evolution of the contact pressure build-up at the borehole for the three simulations.

5.2 Parametric analysis

Next we report results of a parametric study conducted to provide insight into the main factors affecting the contact between the shale and the casing. We focus in particular on the dependence of three quantities on the problem parameters, namely: (i) asymptotic pressure $\tilde{\sigma}_r^\infty$ on the casing or increment $\Delta\tilde{\sigma}_r^\infty = \tilde{\sigma}_r^\infty - \tilde{p}_m$; (ii) contact time τ_c, which is the time elapsed between drilling and first contact between the rock and the casing; and (iii) asymptotic time τ_a, which is the time needed to reach 95% of the asymptotic state, or alternatively $\Delta\tau = \tau_a - \tau_c$, a measure of the time needed for the contact pressure to increase from $\tilde{p}_m$ to the 95% of the final value $\tilde{\sigma}_r^\infty$.

5.2.1 Contact pressure

First consider the possible influence of mud pressure $\tilde{p}_m$ on the asymptotic pressure $\tilde{\sigma}_r^\infty$ acting on the rigid casing. For these simulations, $\tilde{\sigma}_0 = 8.33$ (instead of $\tilde{\sigma}_0 = 5$ used in the benchmark simulations) to enable exploring a relatively large range of values for $\tilde{p}_m$ causing failure of the rock around the borehole. Fig. 17 shows both $\tilde{\sigma}_r^\infty$ and $\Delta\tilde{\sigma}_r^\infty$ as functions of $\tilde{p}_m \in [0, 1.46]$. It can be seen that $\tilde{\sigma}_r^\infty$ depends only slightly on $\tilde{p}_m$, noting that additional unloading takes place with increasing shrinkage of the viscoplastic annulus at lower $\tilde{p}_m$. This result is confirmed by Fig. 18 illustrating the evolution of the thickness $\delta(\tau)$ of the viscoplastic annulus for several values of mud pressure $\tilde{p}_m \in [0, 1.46]$. While the initial value $\delta(0^+)$ of the annulus thickness, given by (55), indeed depends on $\tilde{p}_m$, the large time asymptotic value $\delta(\infty)$ is slightly influenced by this parameter. In fact, $\delta(\infty)$ can be approximated reasonably well by the elastoplastic solution δ_p, obtained by solving $\tilde{u}_p(0) + \omega = 0$ with the displacement at the borehole wall evaluated according to the classic elastoplastic solution (75). Fig. 18 confirms the good match between $\delta(\infty)$ and δ_p (here $\delta_p = 0.502$ and represented by the dashed line).

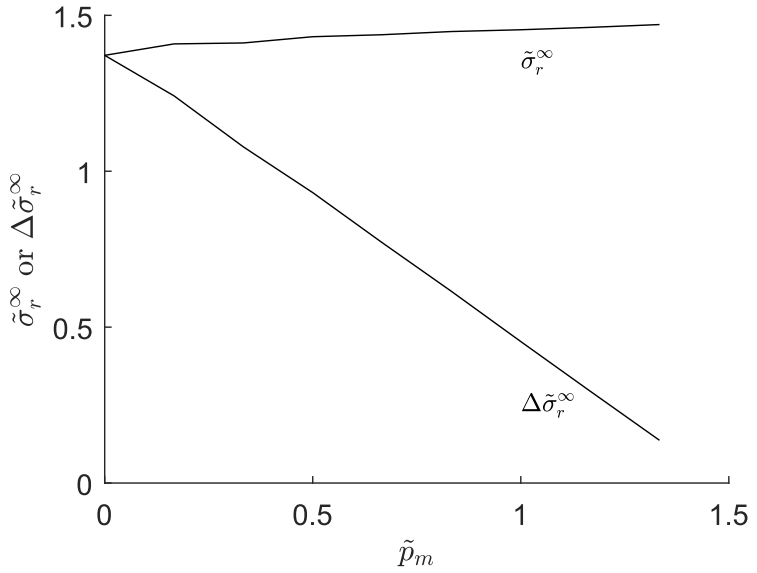

Figure 17: Asymptotic contact pressure $\tilde{\sigma}_r^\infty$ and its increment $\Delta\tilde{\sigma}_r^\infty$ after contact with respect to the initial borehole pressure $\tilde{p}_m$.

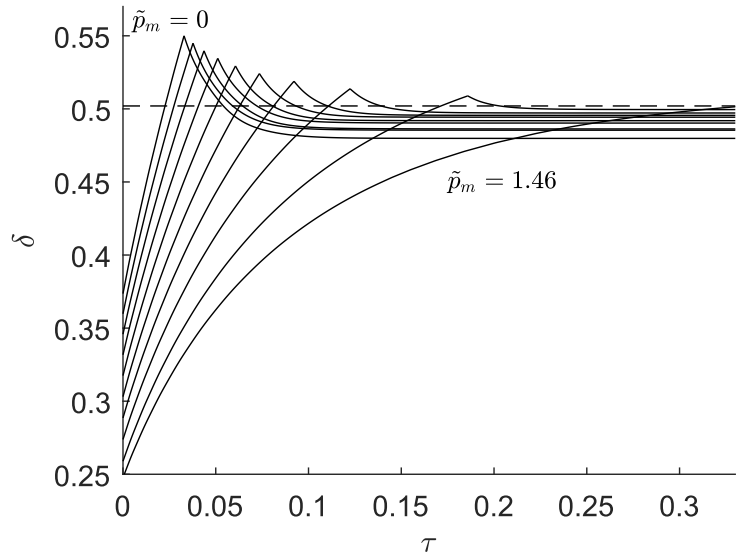

Figure 18: The evolution of the thickness $\delta(\tau)$ of the viscoplastic annulus at different initial borehole pressure $\tilde{p}_m$. From the severest to the mildest evolution of the viscoplastic annulus, $\tilde{p}_m$ increases from 0 to 1.33 with increment 0.167. The evolution of the viscoplastic annulus with $\tilde{p}_m = 1.46$ indicates the situation $\delta(\tau)$ approaching to the δ_p without contact. Dash – the width of the viscoplastic annulus predicted by the elastoplastic solution.

Furthermore, the large time contact pressure $\tilde{\sigma}_r^{\infty}$ for the viscoplastic model is also well approximated by its elastoplastic counterpart $\tilde{\sigma}_{rp}$, which is deduced from δ_p using (76) with $\tilde{p}_m$ interpreted as $\tilde{\sigma}_{rp}$ ($\tilde{\sigma}_{rp} = 0$ for the set of parameters used for the simulations). The good match between these two quantities is confirmed in Fig. 19, where both $\tilde{\sigma}_r^{\infty}$ and $\tilde{\sigma}_{rp}$ are plotted versus $\tilde{\sigma}_0$. Figure 19 also indicates that for far-field stress below the threshold $\tilde{\sigma}_0 = 3.53$, there is no contact pressure build-up as the casing annulus remains open.

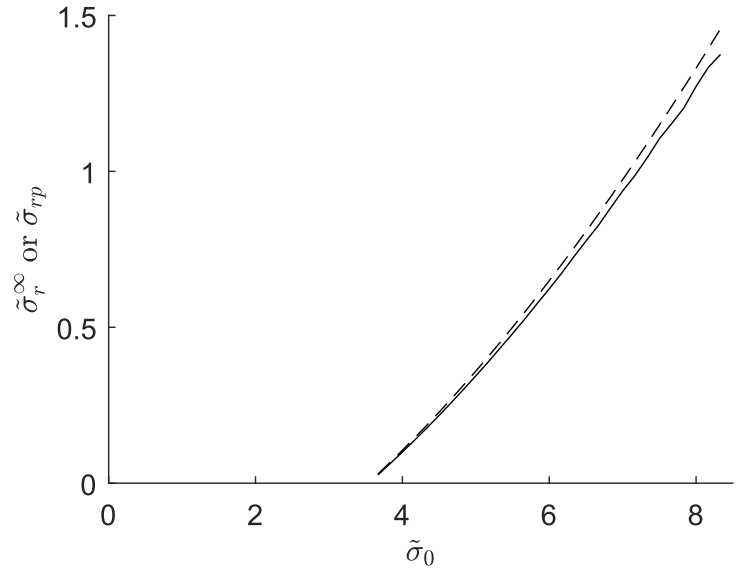

Figure 19: Contact pressure predicted by the viscoplastic model (asymptotic solution $\tilde{\sigma}_r^{\infty}$) and by the elastoplastic model ($\tilde{\sigma}_{rp}$) with respect to in-situ stress. Solid – $\tilde{\sigma}_r^{\infty}$; Dash – $\tilde{\sigma}_{rp}$.

Although practically negligible, there is a difference between the large time viscoplastic solution and the elastoplastic response. The latter solution is constructed on the assumption of monotonic loading and thus of monotonic growth of the plastic region with the loading parameter. On the other hand, as clearly seen in the plot of $\delta(\tau)$ shown in Fig. 18, the sign reversal in the rate of change of $\delta(\tau)$ following contact between the rock and the casing implies elastic unloading in the viscoplastic response. However, the relatively small backward movement of the interface seen in Fig. 18 indicates that the

plastic strain accumulated in the region where elastic unloading takes place is indeed small. Hence the elastoplastic solution corresponding to $\tilde{u}_p(0) + \omega = 0$ is expected to provide a good approximation of the long-term viscoplastic solution.

The above observations have interesting consequences regarding the dependence of $\tilde{\sigma}_r^\infty \simeq \tilde{\sigma}_{rp}$ on the problem parameters. Since the link between $\tilde{\sigma}_r^\infty$ and $\tilde{\sigma}_0$ is legislated by $\delta_\infty \simeq \delta_p(\omega, \nu, k, k_f)$, we can conclude that $\tilde{\sigma}_r^\infty \simeq \tilde{\sigma}_{rp}(\tilde{\sigma}_0, \omega, \nu, k, k_f)$. This implies that the elastic modulus and strength of the rock only affect $\tilde{\sigma}_r^\infty$ only via $\tilde{\sigma}_0$ and the dimensionless gap ω, which takes value only in the narrow range $[0.9 \sim 3.8]$.

5.2.2 Contact Time and Asymptotic Time

Figure 20 and 21 show the variation of contact time τ_c and asymptotic time τ_a with $\tilde{\sigma}_0$ and $\tilde{p}_m$, respectively. Both τ_c and τ_a decrease with $\tilde{\sigma}_0$ but increase with $\tilde{p}_m$. These trends reflect the larger overstress and thus the larger viscoplastic strain rate associated with a larger $\tilde{\sigma}_0$ and/or a smaller $\tilde{p}_m$. However, neither $\tilde{\sigma}_0$ nor $\tilde{p}_m$ appear to affect the time interval $\Delta\tau = \tau_a - \tau_c$, which gives a measure of the time needed to reach the equilibrium state. Although there is no formal proof as to why $\Delta\tau$ would be insensitive to $\tilde{\sigma}_0$ and $\tilde{p}_m$, we note that a larger overstress state at the moment of contact indicates a longer path to return to zero. On the other hand, a larger overstress is also responsible for a quicker return. These two effects compete, apparently balancing each other so that $\Delta\tau$ hardly depends on $\tilde{\sigma}_0$ and $\tilde{p}_m$.

A parametric analysis shows that $\Delta\tau$ is essentially a function of the dimensionless shear modulus γ (Fig. 22), k and k_f.

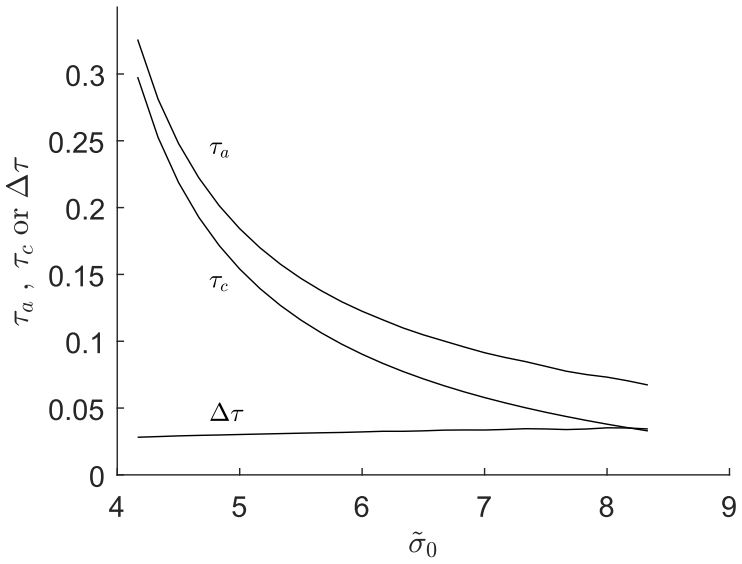

Figure 20: Time duration of contact, asymptotic solution, and the increment affected by in-situ stress, assuming $\tilde{p}_m = 0$.

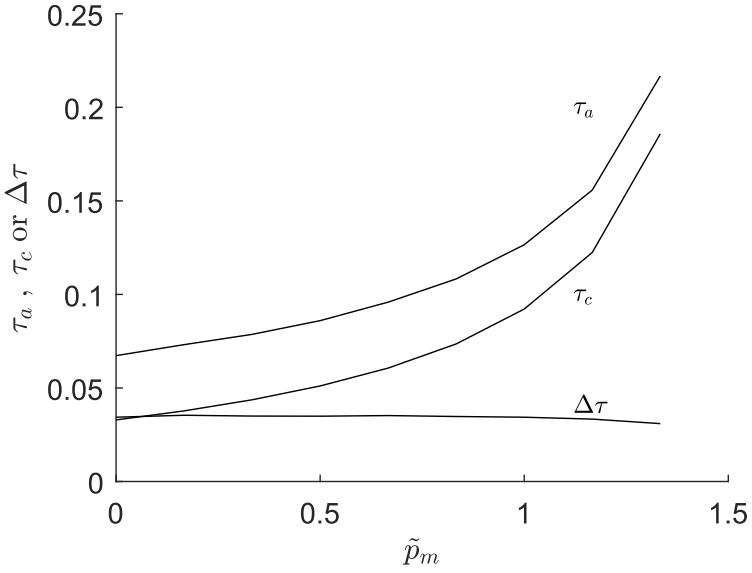

Figure 21: Time duration of contact, asymptotic solution, and the increment affected by initial borehole pressure, assuming $\tilde{\sigma}_0 = 8.33$.

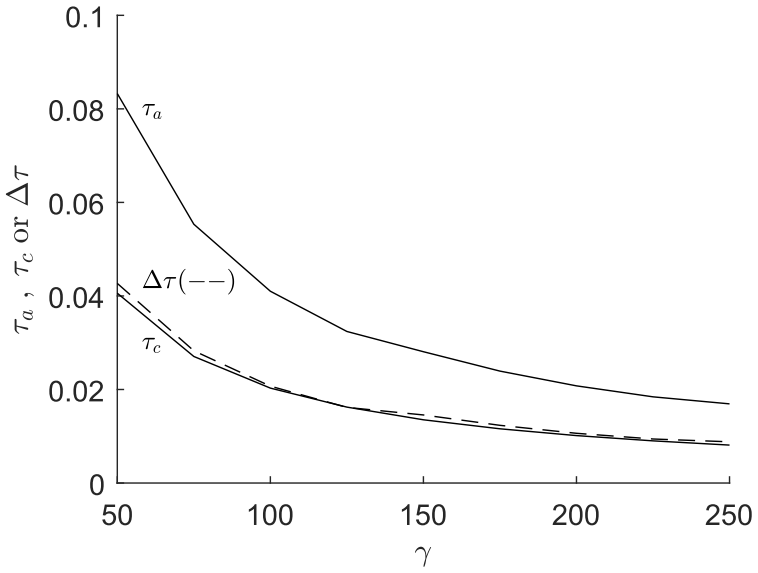

Figure 22: Time duration for contact, asymptotic solution, and the increment affected by γ (changing G), assuming $q = 6\,\mathrm{MPa}$.

6 Conclusions

This paper has described a model to predict and analyze the time-dependent closure of a borehole drilled in a soft rock, as well as the build-up of stress on a rigid casing, once the rock contacts the casing. The rock is assumed to behave as a viscoplastic material in the spirit of Perzyna's [1966] original theory, which allows the stress to temporarily violate the yield criterion. Here a Mohr-Coulomb yield criterion and a plastic potential are adopted and the stress-strain deviatoric response is akin to a Bingham rheological model.

With the simplifying hypotheses of plane strain and axisymmetry, the latter one linked to the assumption of an isotropic far-field stress, the field quantities only depend on two independent variables, radial coordinate r and time t. Furthermore, the model formulation recognizes the particular structure of the solution, namely that the borehole is encircled by an evolving viscoplastic annulus, itself surrounded by an infinite domain,

where the rock is either elastic or is unloading elastically. Noting that the solution outside the viscoplastic boundary is given explicitly by the Lamé solution, the evolution problem is formulated as an initial boundary value problem in the viscoplastic region only, but with a free boundary — the growing or shrinking interface between the viscoplastic and elastic domains. In other words, our formulation involves explicit tracking of that interface.

This work has demonstrated how the mathematical framework and the computational algorithm with a moving mesh can efficiently solve this class of problems. The set of equations governing the mechanical fields and the evolution of viscoplastic boundary is transformed by mapping the viscoplastic annulus to the interval $[0, 1]$, resulting in the replacement of radius r with moving coordinate χ as the independent spatial variable. These new equations can then be spatially discretized on a moving mesh with a fixed number of nodes. The final system of equations are first order ODEs that express the rate of change of the state variables defined at the nodes of the mesh and the velocity of the interface. This set of ODE is solved numerically using the MATLAB routine ODE45. The high accuracy of the numerical solution has been confirmed by demonstrating that the long-term solution, when the borehole pressure remains constant following unloading due to drilling, matches the classical elastoplastic solution.

Numerical simulations based on the viscoplastic constitutive model indicate that some reverse movement of the elasto-viscoplastic interface occurs once the rock contacts the rigid casing, which is evidence of the development of an intermediate ring in between the elastic and the viscoplastic region. In this ring, the rock experiences elastic unloading. In fact, the final contact pressure reached when the viscoplastic strain rate field has vanished is given to a good approximation by the classical elastoplastic solution corresponding to an imposed borehole displacement consistent with the presence of a rigid casing.

The time taken for the deforming rock to contact the casing following drilling is of order $O\left(0.1T \sim 1T\right)$ with T denoting the characteristic time $T = \eta/q$; it decreases with

the higher in-situ stress σ_0/q but increases with the higher mud pressure p_m/q. Noting that the relative gap between the borehole wall and the casing is practically fixed, the effective duration of the stress build-up on the casing is of order $O\left(0.01T\right)$ and appears to be affected mainly by rock properties (the ratio G/q, the friction angle ϕ and the dilation angle ψ) and to be insensitive to σ_0/q and p_m/q.

The above results are evidently tied to the assumed constitutive response of the rock. Laboratory experiments should be conducted to assess the adequacy of this constitutive representation or to develop a more realistic model of the time-dependent response of shales. Nonetheless, the mathematical framework and the algorithmic procedure described in this paper are the foundations of fast and accurate computer codes that can readily be modified to include additional features of the constitutive response. The numerical simulations presented here would hopefully still remain useful as simple benchmarks for software based on the finite element method or related methods.

7 Acknowledgement

This work was sponsored by The Research Council of Norway, Aker BP, BP, ConocoPhillips, Equinor, Shell, and Total, through the PetroMaks 2 KPN-project: Shale as a Permanent Barrier after Well Abandonment, at SINTEF Industry (Grant no. 244420/E30).

References

G. Barla, D. Debernardi, and D. Sterpi. Time-dependent modeling of tunnels in squeezing conditions. *International Journal of Geomechanics*, 12(6):697–710, dec 2012. doi: 10.1061/(asce)gm.1943-5622.0000163.

H. Bian, X. Zhang, and J. Shao. A coupled elastoplastic and visco-plastic damage model for hard clay and its application for the underground gallery excavation. *Underground Space*, 2(1):60–72, mar 2017. doi: 10.1016/j.undsp.2017.03.002.

E. C. Bingham. *Fluidity and Plasticity*, volume 2. McGraw-Hill, 1922.

E. Boidy. *Modélisation numérique du comportement différé des cavités souterraines*. PhD thesis, Université Joseph-Fourier - Grenoble I, 2002.

E. Boidy, A. Bouvard, and F. Pellet. Back analysis of time-dependent behaviour of a test gallery in claystone. *Tunnelling and Underground Space Technology*, 17(4):415–424, oct 2002. doi: 10.1016/s0886-7798(02)00066-4.

M. Bonini, D. Debernardi, M. Barla, and G. Barla. The mechanical behaviour of clay shales and implications on the design of tunnels. *Rock Mechanics and Rock Engineering*, 42(2):361, Oct 2007. ISSN 1434-453X. doi: 10.1007/s00603-007-0147-6.

N. Cristescu. Viscoplastic creep of rocks around a lined tunnel. *International Journal of Plasticity*, 4(4):393 – 412, 1988. ISSN 0749-6419. doi: 10.1016/0749-6419(88)90026-5.

D. Debernardi. *Viscoplastic behaviour and design of tunnels*. PhD thesis, Politecnico di Torino, 2008.

E. Detournay. Elastoplastic model of a deep tunnel for a rock with variable dilatancy. *Rock Mechanics and Rock Engineering*, 19(2):99–108, 1986.

E. Fjaer, R. M. Holt, A. Raaen, R. Risnes, and P. Horsrud. *Petroleum related rock mechanics*, volume 53. Elsevier, 2008.

P. Fritz. An analytical solution for axisymmetric tunnel problems in elasto-viscoplastic media. *International Journal for Numerical and Analytical Methods in Geomechanics*, 8(4):325–342, jul 1984. doi: 10.1002/nag.1610080403.

G. Gioda. On the non-linear 'squeezing' effects around circular tunnels. *International Journal for Numerical and Analytical Methods in Geomechanics*, 6(1):21–46, jan 1982. doi: 10.1002/nag.1610060104.

G. Gioda and A. Cividini. Numerical methods for the analysis of tunnel performance in squeezing rocks. *Rock Mechanics and Rock Engineering*, 29(4):171–193, Oct 1996. ISSN 1434-453X. doi: 10.1007/BF01042531.

K. Hashiguchi. Viscoplastic constitutive equations. In *Foundations of Elastoplasticity: Subloading Surface Model*, pages 415–429. Springer International Publishing, 2017. doi: 10.1007/978-3-319-48821-9-13.

J. Lemaitre and J.-L. Chaboche. *Mechanics of solid materials*. Cambridge University Press, 1990. doi: 10.1017/cbo9781139167970.

D. F. Malan. Time-dependent behaviour of deep level tabular excavations in hard rock. *Rock Mechanics and Rock Engineering*, 32(2):123–155, may 1999. doi: 10.1007/s006030050028.

M. H. Moghadam. A numerical analysis of wellbores in shale with viscoplastic behavior. In *47th US Rock Mechanics/Geomechanics Symposium*. American Rock Mechanics Association, 2013.

D. Norsok. D-010. well integrity in drilling and well operations. *Standards Norway, Rev*, 4, 2013.

P. Perzyna. Fundamental problems in viscoplasticity. In G. Chernyi, H. Dryden, P. Germain, L. Howarth, W. Olszak, W. Prager, R. Probstein, and H. Ziegler, editors, *Advances in Applied Mechanics*, volume 9 of *Advances in Applied Mechanics*, pages 243–377. Elsevier, 1966. doi: 10.1016/s0065-2156(08)70009-7.

S. M. Williams, T. Carlsen, K. C. Constable, A. C. Guldahl, et al. Identification and qualification of shale annular barriers using wireline logs during plug and abandonment operations. In *SPE/IADC Drilling Conference and Exhibition*. Society of Petroleum Engineers, 2009.

Appendix – Convergence analysis

To assess the convergence rate of the algorithm, the relative error between the large time displacement at the borehole if the absence of a casing and the elastoplastic solution, has been calculated for various grid densities,

$$\text{error} = \frac{1}{n}\sqrt{\sum_{i=1}^{n}\left|\frac{\tilde{u}\left(\chi_i,\infty\right)-\tilde{u}_p\left(\chi_i\right)}{\tilde{u}_p\left(\chi_i\right)}\right|^2} \tag{77}$$

Fig. 23 illustrates the error as a function of the number of grid points. As can be observed on this plot, the convergence rate of the algorithm is about 2.

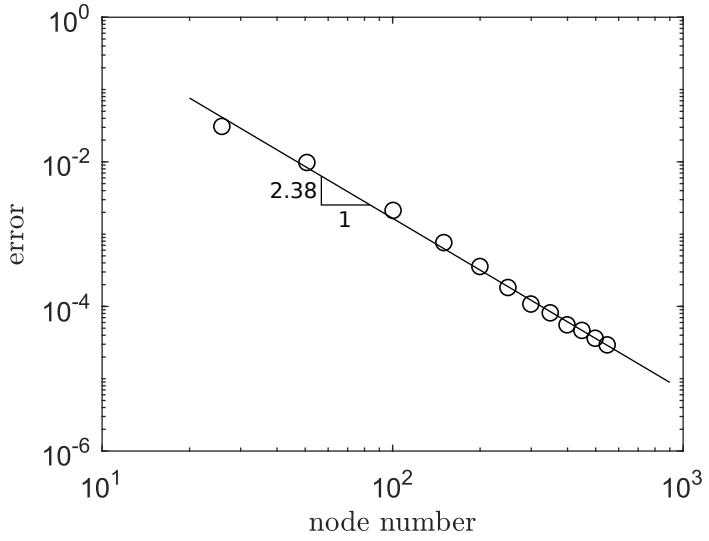

Figure 23: Variation of error with number of grid points